Highly sensitive sensor based on 4×4 multimode interference coupler with microring resonators

TRUNG-THANH LE*
International School (VNU-IS), Vietnam National University (VNU), Hanoi, Vietnam

This study proposes a novel optical integrated structure using only one 4x4 multimode interference (MMI) coupler with support of two microring resonators for glucose and ethanol sensor. Due to the presence of the analyte, the wavelength shift of the output spectrum is realized. The proposed structure can provide a high sensitivity of 721 nm/RIU, low detection limit of $2.8x10^{-5}$ and good figure of merit of $5x10^{16}$ for glucose sensing.

(Received June 12, 2017; accepted June 7, 2018)

Keywords: Glucose sensor, Multimode interference, Microring resonator, Integrated optics

1. Introduction

Optical sensors have been used widely in many applications such as biomedical research, healthcare and environmental monitoring [1]. In general, detection can be made by the optical absorption of the analytes, optic spectroscopy or the refractive index change. The two former methods can be directly obtained by measuring optical intensity. The third method is to monitor various chemical and biological systems via sensing of the change in refractive index [2, 3]. A number of refractive index sensors based on optical waveguide structures have been proposed such as Bragg grating sensors, directional coupler sensors, Mach- Zehnder interferometer (MZI) sensors, microring resonator sensors and surface plasmon resonance sensors [4].

In recent years, optical microring resonators are becoming versatile components for communication and sensing applications. Many optical devices based on microring resonators such as optical filters, optical multiplexers and optical switches have been reported [5]. Optical sensors based on microring resonators have attracted considerable attention due to their compactness and high sensitivity. However, only optical sensors using microring resonators based on 2×2 directional couplers or 2×2, 3×3 multimode interference (MMI) couplers have been reported [6].

Multimode interference can be a versatile structure for optical applications. There are a variety functional devices based on MMI structures such as optical variable splitter [7], filter [8], multiplexing [9], mode multiplexing [10], switch [11], modulator [12], fast and slow light [13], Fano shape generation [14], logic gates [15], sensor [16], optical transforms [17], etc.

Gas detection is developed for miniaturization use various principles such as electrochemical, catalytic or optical detection [18]. Optical sensors advantages of operating at room temperature and requiring no electrical connections. In addition, Silicon on Insulator (SOI) was recently proved to be a viable technology for a wide range of integrated optical applications, from optical devices, optical interconnects to biosensors [19]. The SOI devices have ultra-small bends due to its high refractive index contrast and are compatible with the existing CMOS (Complementary Metal-Oxide-Semiconductor) fabrication technologies. This has attracted much attention for realizing ultra-compact and cheap optical sensors.

In recent years, a double Fano structure based on 4×4 MMI coupler has been studied. It is showed that MMI based sensors have advantages of compactness, large fabrication tolerance, small insensitivity to temprature fluctuation and ease of fabrication [20].

In this study, a novel optical sensor structure based on only one 4×4 MMI coupler integrated with two microring resonators (MRRs) is further analyzed, developed and proposed [21]. The structure can generate the Fano line shape and therefore can provide a very high sensitivity, low detection limit (DL) and a good figure of merit (FOM). As an example, the proposed structure is applied to glucose and ethanol sensing applications.

2. Sensor structure based on 4x4 MMI coupler and two microring resonators

A schematic of the structure is shown in Fig. 1(a). The proposed structure contains one 4×4 MMI coupler, where a_i, b_i (i=1,...,4) are complex amplitudes at the input and output waveguides. Two microring resonators are used in two output ports. In our design, the silicon waveguide with a height of 220 nm, width of 500 nm is used for single mode operation. The wavelength is at 1550 nm. The silica is used for cladding cover at the reference resonator. The analyte is used as cladding at the sensing region. The field profile of the waveguide is shown in Fig. 1(b) calculated by finite difference method (FDM) [22]. The refractive

index of silicon material is calculated by using the Sellmeier equation [23]:

$$n^2(\lambda) = \varepsilon + \frac{A}{\lambda^2} + \frac{B\lambda_1^2}{\lambda^2 - \lambda_1^2} \quad (1)$$

where $\varepsilon = 11.6858$, A=0.939816μm^2, B=8.10461x10^{-3} and $\lambda_1 = 1.1071\mu m$. The refractive index of silicon for wavelength from 1550 nm to 1600 nm is shown in Fig. 2. At wavelength $\lambda = 1550nm$, the refractive index of silicon is 3.455. For silica material, the refractive index is nearly a constant of 1.444 for the given wavelength range [24].

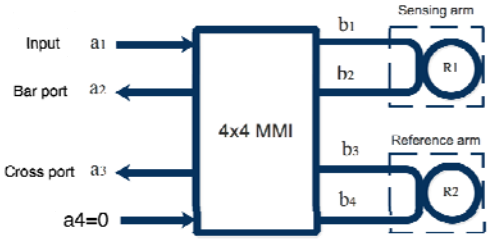

(a)

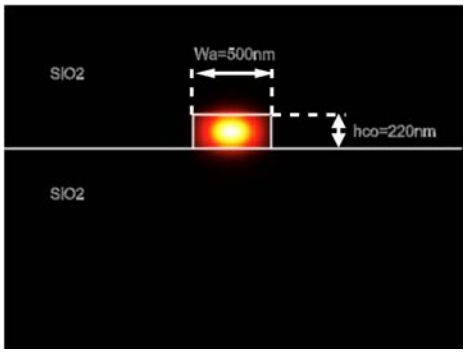

(b)

Fig. 1(a). Schematic diagram of a 4x4 MMI coupler based sensor where input port $a_4 = 0$ with no input signal and (b) Waveguide structure profile with height of 220nm and width of 500 nm for TE (transverse electric) mode

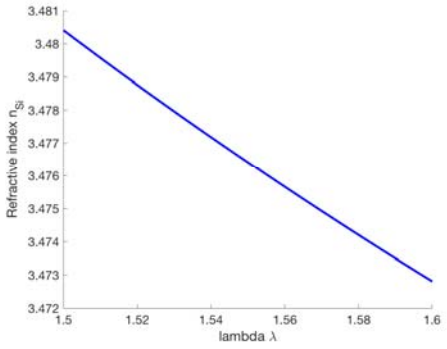

Fig. 2. Refractive index of silicon for wavelenth from 1500 nm to 1600 nm

It was shown that this structure can create Fano resonance, CRIT (coupled resonance induced transparency) and CRIA (coupled resonance induced absorption) at the same time [25]. The Fano line shape by changing the radius R_1 and R_2 or the coupling coefficients of the couplers used in microring resonators can be changed. Here, microring resonator with radius R_1 is used for sensing region and microring with R_2 for reference region. The analyte will be covered around the cladding of the optical waveguide and therefore causing the change in effective refractive index and output spectrum of the device. By measuring the shift of the resonance wavelength, the concentration of the glucose and ethanol can be determined.

In this paper, the access waveguides are identical single mode waveguides with width W_a. The input and output waveguides are located at positions [26]:

$$x = (i + \frac{1}{2})\frac{W_{MMI}}{N}, \text{ (i=0,1,…,N-1)} \quad (2)$$

where N is the number of output ports. By using the analytic and numerical methods, it is shown that at these positions of input waveguides and the length of 4x4 MMI coupler of $L_{MMI} = \frac{3L_\pi}{2}$, the 4x4 MMI coupler acts as two 3dB (50:50) couplers [27].

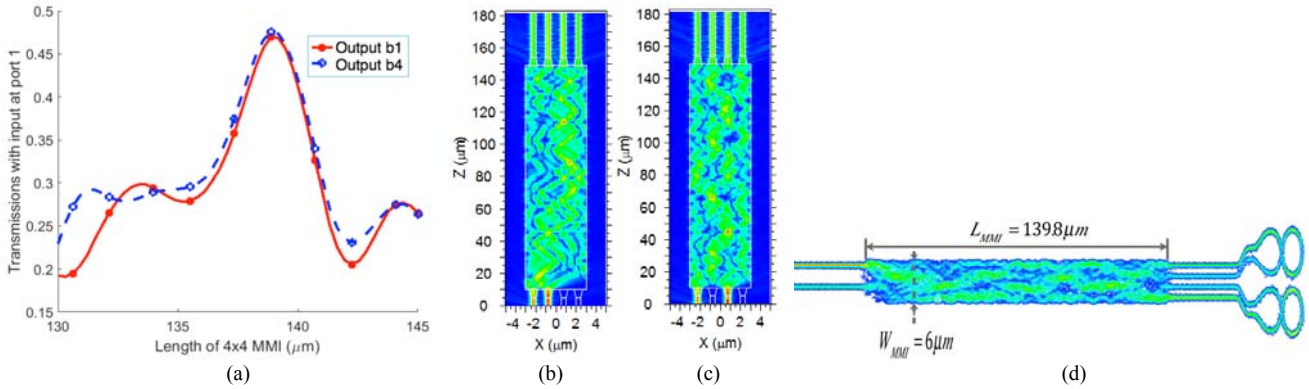

(a) (b) (c) (d)

Fig. 3(a). Transmissions at the bar and cross ports of the 4x4 MMI coupler; (b) power transmission through the 4x4 MMI at the optimized length 138.9 μm *when input signal is at port* a_1 *and phase difference between two arm lengths of 180 degrees; (c) power transmission through the 4x4 MMI when input signal is at port* a_1 *and phase difference of 0 degree and (d) transmissions through the whole device with the presence of two microring resonators*

In order to create a compact device, it is showed that the width of the MMI is optimized to be W_{MMI}=6μm. The calculated length of each MMI coupler is found to be $L_{MMI} = 138.9$ μm as shown in Fig. 3(a) when input signal is at port a_1. Fig. 3(b) and (c) show the transmission through the structure when the phase difference between two arms of 0 and 180 degree. It is assumed that the signal is at input port a_1. When signal is presented at input port a_2 or a_3, the device behaviour is similar to that of input port a_1 or a_4. Without loss of generality, only input port a_1 for input signal is used. Input port a_4 can also be used for input port equivalently to input port 1 as shown in Fig. 3(d) by using finite difference time difference (FDTD) with a grid size $\Delta x = \Delta y = \Delta z = 20nm$ [28].

In this study, homogeneous sensing mechanism is used, where κ_1 and τ_1 are the cross coupling coefficient and transmission coupling coefficient of the coupler 1; α_1 is the loss factor of the field after one round trip through the microring resonator; $\varphi_1 = 2\pi n_{eff} L_{R_1} / \lambda$ is the round trip phase, n_{eff} is the effective index and L_{R1} is the microring resonator length.

The design procedure of the coupler parameters used for microring resonators to achieve the required coupling coefficients are similar to that presented in the recent work [13]. In this study, a gap of 90 nm for 3dB coupling is used.

The normalized transmitted power at the output waveguide is [29]:

$$T_1 = \left|\frac{b_2}{b_1}\right|^2 = \frac{\alpha_1^2 - 2\alpha_1\tau_1\cos(\varphi_1) + \tau_1^2}{1 - 2\alpha_1\tau_1\cos(\varphi) + \alpha_1^2\tau_1^2} \quad (3)$$

When light is passed through the input port of the microring resonator, all of the light are received at the through port except for the wavelength which satisfies the resonance conditions:

$$m\lambda_r = n_{eff} L_{R_1} = n_{eff}(\pi R_1) \quad (4)$$

$$m\lambda_r = n_{eff} L_{R_2} = n_{eff}(\pi R_2) \quad (5)$$

where λ_r is the resonance wavelength and m is an integer representing the order of the resonance. The operation of the sensor using microring resonators is based on the shift of resonance wavelength. A small change in the effective index n_{eff} will result in a change in the resonance wavelength. The change in the effective index is due to a variation of ambient refractive index (n_a) caused by the presence of the analytes in the microring. The sensitivity of the microring resonator sensor is defined as [16, 30]

$$S = \frac{\partial\lambda_r}{\partial n_a} = \frac{\partial\lambda_r}{\partial n_{eff}}\frac{\partial n_{eff}}{\partial n_a} = \frac{\partial\lambda_r}{\partial n_{eff}}(S_W)[\text{nm/ RIU}] \quad (6)$$

where $S_W = \frac{\partial n_{eff}}{\partial n_a}$ is the waveguide sensitivity, that depends only on the waveguide design and is a constant for a given waveguide structure. RIU is refractive index unit.

Another important figure of merit for sensing applications is the detection limit (DL) δn_a. It can be defined as

$$DL = \delta n_a \approx \frac{\lambda_r}{SQ} \approx \frac{R_{OSA}}{S}[\text{RIU}] \quad (7)$$

where Q is the quality factor of the microring resonator, R_{OSA} is the resolution of optical spectral analyzer [29, 31, 32]. It is desirable to have a small refractive index resolution, in which a small ambient index change can be detected. Therefore, high Q factor and sensitivity S are necessary.

The effect of ring radius on the sensing performance is now investigated; the ratio of the two ring radii is defined as $a = \frac{R_2}{R_1}$, where a<1. The sensitivity of the proposed sensor is calculated by

$$S = \frac{\lambda_{shift}}{\Delta n_a} = \frac{1}{1-a}\frac{\Delta\lambda}{\Delta n_a} \quad (8)$$

$$LOD = \frac{\Delta n_{eff}}{n_{eff}} = \frac{1-a}{a}\frac{\lambda}{2\pi R_2 n_{eff}} \quad (9)$$

It is obvious that the sensitivity of the proposed structure is 1/(1-a) times than that of a sensor based on single microring resonator [33]. When the ratio factor $a = \frac{R_2}{R_1}$ approaches unity, the sensitivity of the proposed structure is much higher than that of the conventional one as shown in Fig. 4.

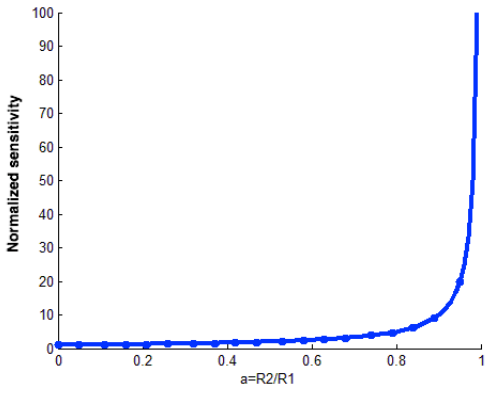

Fig. 4. Comparison of sensivity of the proposed structure with the sensitivity of the single microring sensor at different ratio between two ring radii

After some calculations, the transmissions at the output port 2 (bar port) and 3 (cross port) of Fig.1 are given by

$$T\_bar = \left|\cos(\frac{\Delta\varphi}{2})\right|^2 \quad (10)$$

$$T\_cross = \left|\sin(\frac{\Delta\varphi}{2})\right|^2 \quad (11)$$

The transmissions of the bar and cross ports are shown in Fig. 5, where $R_1 = 10\mu m$ and a=0.5. The simulations show that the Fano resonance can be achieved. It has been suggested that optical Fano resonances have many important applications in highly sensitive chemical and biological sensing, optical switching, modulating and filtering [34, 35]. It is because the sensitivity of the sensor based on this structure can be greatly enhanced by steeping the slope of the transmission.

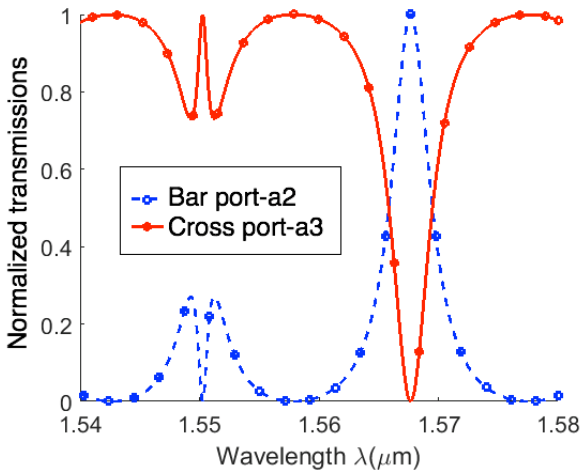

Fig. 5. Transmissions at the bar and cross ports of the proposed sensor structure in Fig. 1

3. Simulation results and discussions

The refractive index of the glucose (n) can be calculated from the glucose concentration (C%) by [20]

$$n = 0.2015x[C] + 1.3292 \quad (12)$$

The refractive index of the glucose is shown in Fig. 5. By using the finite difference method (FDM), the effective refractive index of the waveguide at different glucose concentration is shown in Fig. 6.

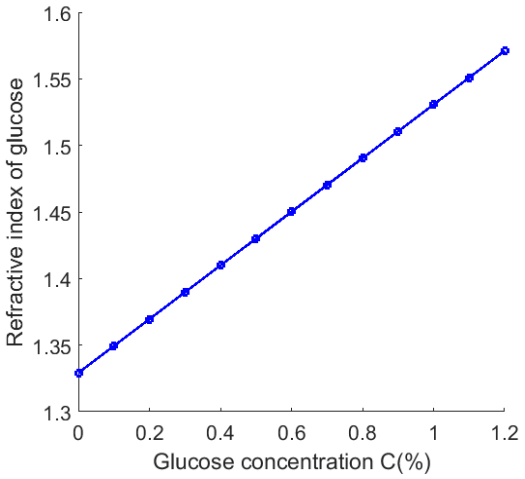

Fig. 6. Refractive index of the glucose verus concentation

Now the behavior of our devices is investigated when the radius of two microring resonators is different. For example, the radii of microring resonators $R_1 = 20\mu m$ and $R_2 = 10\mu m$, loss factor a=0.5 and $\alpha_1 = \alpha_2 = 0.98$ are chosen, respectively. It is assumed that 3dB couplers are used at the microring resonators 1 and 2. The glucose solutions with concentrations of 0%, 0.2% and 0.4% are induced to the device. Fig. 7 shows the effective refractive index of the waveguide calculated by the FDM with different glucose concentration. Here the electrical field profile when C=0% and 1.2% is presented.

The resonance wavelength shifts corresponding to the concentrations can be measured by the optical spectrometer as shown in Fig. 8 and Fig. 9. For each 0.2% increment of the glucose concentration, the resonance wavelength shifts of about 800 nm is achieved. This is a double higher order than that of the recent conventional sensor based on single microring resonator [6, 36].

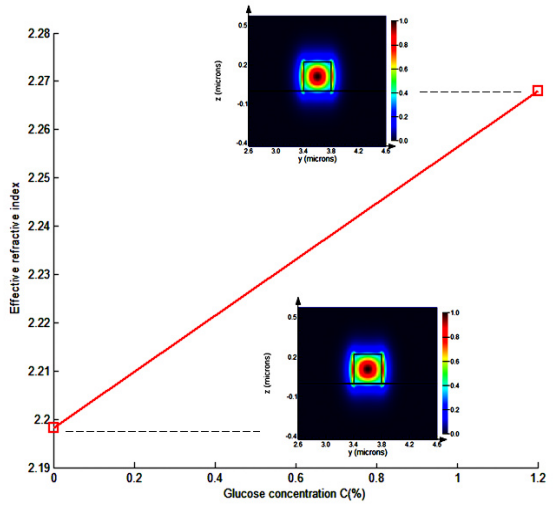

Fig. 7. Effective refractive index at different glucose concentration (field profiles are shown in the boxe with scaled dimensions)

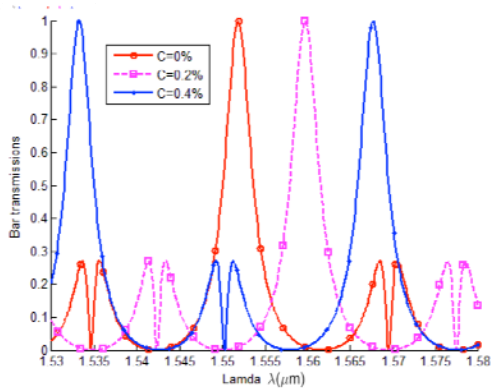

Fig. 8. Transmissions at different glucose concentrations

By measuring the resonance wavelength shift ($\Delta\lambda$), the glucose concentration is detected. The sensitivity of the sensor can be calculated by

$$S = \frac{\Delta\lambda}{\Delta n} = 721 \text{ (nm/ RIU)} \quad (13)$$

Our sensor provides the sensitivity of 721 nm/RIU compared with a sensitivity of 170 nm/RIU [6]. If the optical refractometer with a resolution of 20 pm is used, the detection limit of our sensor is about 2.8×10^{-5}, compared with a detection limit of 1.78×10^{-5} of single microring resonator sensor.

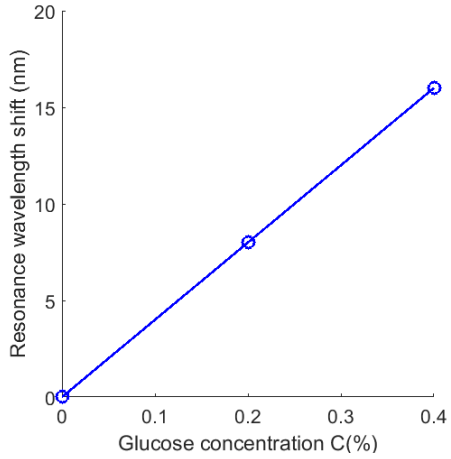

Fig. 9. Resonance wavelength shift at different glucose concentrations

To better evaluate the performance of the proposed sensor, the figure of merit (FOM) is studied. The FOM of the sensor is defined by

$$\text{FOM} = \frac{\Delta T}{(T\Delta n)} \quad (14)$$

Where T is the transmittance at the output of the sensor. The calculated FOM is shown in Fig. 10. It is shown that a very high FOM of 5×10^{16} at wavelength of 1576 nm can be achieved. This FOM value is significantly greater than that of the previous reports [37].

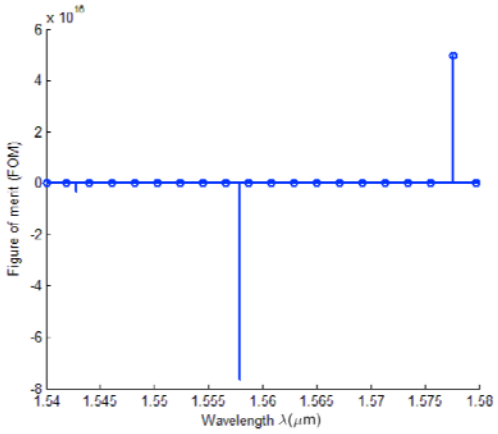

Fig. 10. The FOM at different wavelengths

Next, the proposed structure used for ethanol sensor mechanism is studied. The refractive index of the ethanol ($n_{ethanol}$) can be calculated from the ethanol concentration ($C_{ethanol}$ %) by [20]

$$n_{ethanol} = 1.3292 + a[C_{ethanol}] + b[C_{ethanol}]^2 \quad (15)$$

where $a = 8.4535\times10^{-4}$ and $b = -4.8294\times10^{-6}$. The normalized transmissions at bar port for ethanol concentrations of 0%, 3% and 6% are shown in Fig. 11. The resonance wavelength shifts of the structure at different concentrations of ethanol are shown in Fig. 12. The sensitivity of the ethanol sensor therefore is to be $S_{ethanol} = \frac{\Delta\lambda}{\Delta n} = 200 \text{ (pm/ RIU)}$. It is clear that the sensitivity of the ethanol sensor is much smaller than that of the glucose sensor. As a result, the proposed structure has a better performance for glucose sensing.

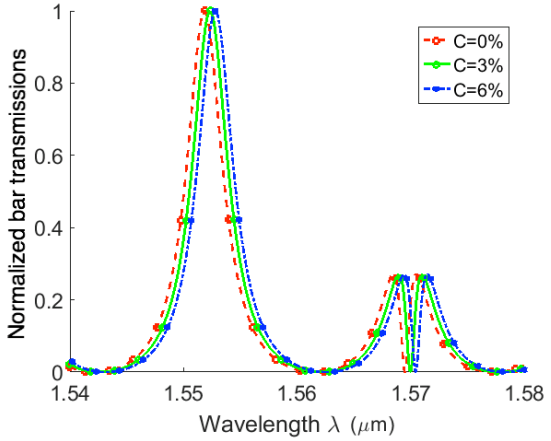

Fig. 11. Transmissions at the bar port for different concentrations of ethanol

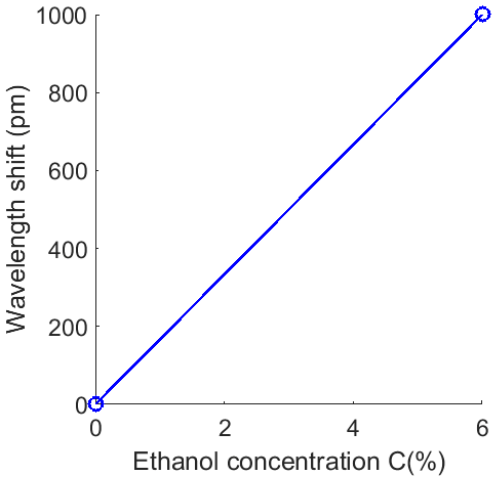

Fig. 12. Wavelength resonance shifts for different concentrations of ethanol

In recent years, for sugar concentration sensing based on MMI couplers, a sensitivity of 169 nm/RIU has been achieved [6]. The proposed sensor can provide a four times higher sensitivity compared to that of the sensor in the literature.

The disadvantage of the proposed sensor comes from the working principle of the sensor based on resonance wavelength shift. Because silicon material is highly sensitive to temperature fluctuations due to a high thermo-optic coefficient (TOC) of silicon ($TOC_{Si} = 1.86x10^{-4} K^{-1}$), the resonance wavelength shift will be affected by the fluctuation of temperature. In order to overcome these fluctuations, some approaches including of both active and passive methods can be used [3]. For example, the local heating of silicon itself to dynamically compensate for any temperature fluctuations, material cladding with negative thermo-optic coefficient, MZI cascading intensity interrogation, control of the thermal drift by tailoring the degree of optical confinement in silicon waveguides with different waveguide widths, ultra-thin silicon waveguides can be used for reducing the thermal drift.

4. Conclusion

This study has presented a new structure for glucose and ethanol sensing based on only one 4×4 MMI coupler. The high sensitivity of 721 nm/RIU and low detection limit of 2.8×10^{-5} can be achieved for glucose and 200 pm/RIU for ethanol sensing. The sensor was designed using silicon waveguide that is cheap and compatible with the current existing CMOS technology.

Acknowledgements

This research is funded by Ministry of Natural Resources and Environment of Vietnam under the project BĐKH. 30/16-20.

References

[1] V. M. N. Passaro, F. Dell'Olio, B. Casamassima, F. D. Leonardis, Sensors **7**(4), 508 (2007).
[2] L. Shi, Y. Xu, W. Tan, X. Chen, Sensors **7**(5), 689 (2007).
[3] T.-T. Le, Photonic Sensors 1-8, DOI: 10.1007/s13320-017-0441-1 (2017).
[4] T. Vo-Dinh, "Biomedical Photonics Handbook", CRC Press, 2003.
[5] D. G. Rabus, "Integrated Ring Resonators – The Compendium", Springer-Verlag, 2007.
[6] O. A. Marsh, Y. Xiong, W. N. Ye, IEEE Journal of Selected Topics in Quantum Electronics **23**(2), 440 (2017).
[7] T.-T. Le, International Journal of Engineering and Technology, Singapore **3**(5), 565 (2011).
[8] T.-T. Le, Journal of Engineering Science & Technology, Malaysia **8**(2), 133 (2013).
[9] V. Prajzler, P. Nekvindová, M. Varga, A. Kromka, Z. Remeš, J. Optoelectron. Adv. Mat. **16**(11-12), 1226 (2014).
[10] R. B. Priti, H. Pishvai Bazargani, Y. Xiong, O. Liboiron-Ladouceur, Optics Letters **42**(20), 4131 (2017).
[11] D. Le, C. Truong, T. Le, Optics Communications **387** 148 (2017).
[12] T. D. Le, N. N. Minh, L. T. Thanh, Journal of Science and Technology on Information and Communications **1**(1), 34 (2017).
[13] D.-T. Le, M.-C. Nguyen, T.-T. Le, Optik - International Journal for Light and Electron Optics **131**, 292 (2017).
[14] T.-T. Le, International Journal of Microwave and Optical Technology **13**(5), 406 (2017).
[15] L. W. Cahill, T. T. Le, 10th International Conference on Transparent Optical Networks (ICTON 2008), Athens, Greece, 2008.
[16] T.-T. Le, International Journal of Information and Electronics Engineering, Singapore **2**, 240 (2011).
[17] T.-T. Le, International Journal of Microwave and Optical Technology (IJMOT), USA **7**(2), 127 (2012).
[18] N. A. Yebo, P. Lommens, Z. Hens, R. Baets, Optics Express **18**(11), 11859 (2010).
[19] M. J. Deen, P. K. Basu, "Silicon Photonics: Fundamentals and Devices", Wiley Series in Materials for Electronic & Optoelectronic Applications, 2012.
[20] T.-T. Le, VNU Journal of Science: Natural Sciences and Technology **34**(1), 119 (2018).
[21] T.-T. Bui, T.-T. Le, 2017 International Conference on Information and Communications (ICIC), Hanoi, Vietnam, 2017.
[22] Y.-C. Chiang, Y.-P. Chiou, H.-C. Chang, Journal of Lightwave Technology **20**(8), 1609 (2002).
[23] E. D. Palik, "Handbook of Optical Constants of Solids", Academic Press, San Diego, CA, 1998.
[24] C. Z. Tan, J. Arndt, Journal of Physics and Chemistry of Solids **61**(8), 1315 (2000).
[25] D.-T. Le, T.-T. Le, International Journal of Computer

Systems (IJCS) **4**(5), 95 (2017).
[26] T.-T. Le, L. Cahill, Optics Communications **301-302**, 100 (2013).
[27] D.-T. Le, T.-D. Do, V.-K. Nguyen, A.-T. Nguyen, T.-T. Le, International Journal of Applied Engineering Research **12**(10), 2239 (2017).
[28] W. Yu, "Electromagnetic Simulation Techniques Based on the FDTD Method", Wiley, New Jersey, 2009.
[29] A. Yariv, Electronics Letters **36**, 321 (2000).
[30] C.-Y. Chao, L. J. Guo, IEEE Journal of Lightwave Technology **24**(3), 1395 (2006).
[31] X. Zhou, L. Zhang, W. Pang, Optics Express **24**(16), 18197 (2016).
[32] J. Hu, X. Sun, A. Agarwal, L. C. Kimerling, Journal of the Optical Society of America B **26**(5), 1032 (2009).
[33] J. H. Wade, R. C. Bailey, Annual Review of Analytical Chemistry **9**(1), 1 (2016).
[34] H. Yi, D. S. Citrin, Z. Zhou, Optics Express **18**(3), 2967 (2010).
[35] K. Y. Hon, A. Poon, Proceedings of SPIE **6101**, Photonics West 2006, Laser Resonators and Beam Control IX, San Jose, California, USA, January 2006.
[36] C. Ciminelli, F. Dell'Olio, D. Conteduca, C. M. Campanella, M. N. Armenise, Optics & Laser Technology **59**, 60 (2014).
[37] Z. Chen, L. Yu, L. Wang, G. Duan, Y. Zhao, J. Xiao, IEEE Photonics Technology Letters **27**(16), 1695 (2015).

*Corresponding author: thanh.le@vnu.edu.vn